Investigating the nanoparticle-protein interactions with Nanoparticle Enhanced Laser Induced Breakdown Spectroscopy signal enhancement

Marcella Dell'Aglio[1,*], Zita Salajkova[2,4], Antonia Mallardi[3,*], Maria Chiara Sportelli[2], Jozef Kaiser[4], Nicola Cioffi[2], Alessandro De Giacomo[1,2]

[1] CNR-NANOTEC, Istituto di Nanotecnologia, c/o Chemistry Department, Via Orabona 4, 70125 Bari, Italy;
[2] Department of Chemistry, University of Bari, and CSGI (Center for Colloid and Surface Science), via Orabona 4, 70125, Bari, Italy
[3] CNR-IPCF, Istituto per i Processi Chimico Fisici, c/o Chemistry Department, Via Orabona 4, 70125 Bari, Italy;
[4] Central European Institute of Technology (CEITEC), Brno University of Technology, Purkyňova 656/123, 612 00 Brno, Czech Republic

Corresponding authors: Marcella Dell'Aglio, *email: marcella.dellaglio@cnr.it*

Antonia Mallardi, *email: a.mallardi@ba.ipcf.cnr.it*

Graphical abstract

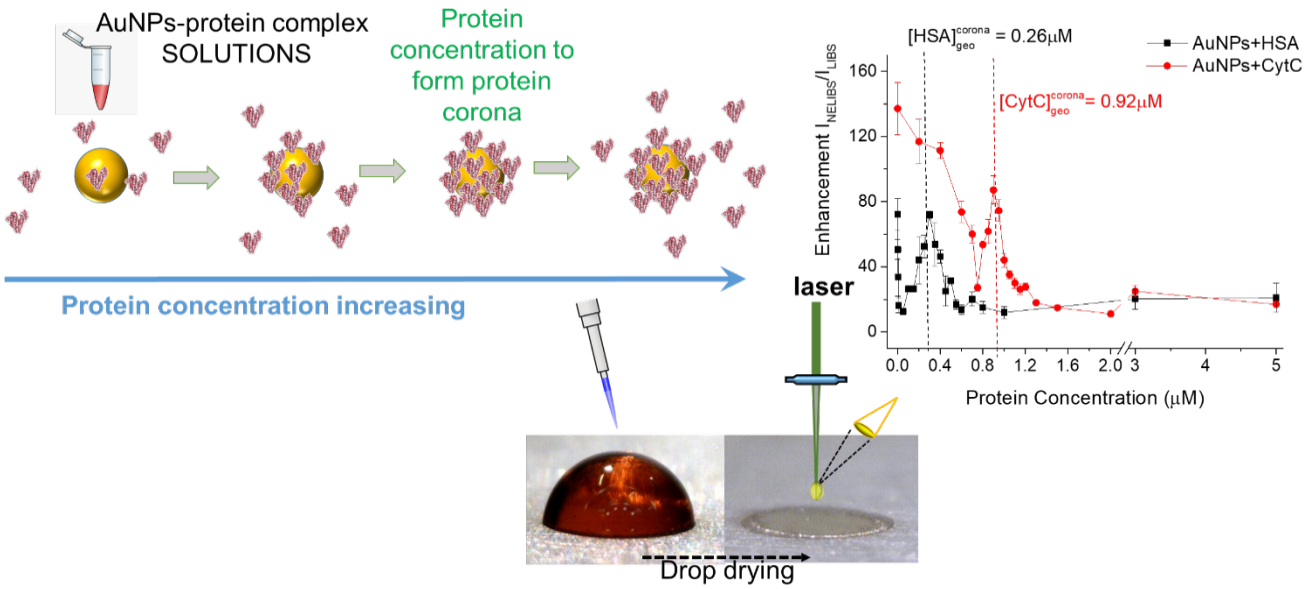

Abstract

Recently Nanoparticle Enhanced Laser Induced Breakdown Spectroscopy (NELIBS) is getting a growing interest as an effective alternative method for improving the analytical performance of LIBS. On the other hand, the plasmonic effect during laser ablation may be exploited for different task rather than traditional elemental analysis.

In this paper the dependence of NELIBS emission signal enhancement on nanoparticle-protein complex on a reference substrate (metallic titanium) has been investigated. Two proteins have been studied and they are Human Serum Albumin (HSA) and Cytochrome C (CytC), having both strong affinity for the gold nanoparticles (AuNPs) due to the bonding between the single free exterior thiol (associated with a cysteine residue) and gold surface to form a long term stable protein corona, but with different number of protein units for the same AuNPs size. The NP-protein complex solution has been dropped and dried on the titanium substrate. Then the NELIBS signal enhancement of Ti emission lines has been correlated to the solution characteristics as determined with Dynamic Light

Scattering (DLS), Surface Plasmon Resonance (SPR) spectroscopy and Laser Doppler Electrophoresis (LDE)- for ζ-potential determination. Moreover, the dried solutions has been studied with TEM (Transmission Electron Microscopy) for the inspection of the inter-particle distance. The structural effect of the NP- protein complex solutions on NELIBS signal reveals that NELIBS can be used to determine the number of protein unities required to form the corona with good accuracy. Although the investigated systems of NP-protein complex are simple cases in biological application, this work demonstrates, for the first time, a different use of NELIBS that is beyond the elemental analysis and it opens the way for sensing the protein corona.

Keywords

NELIBS, gold nanoparticles, nanoparticle protein corona, Human Serum Albumin, Cytochrome C, naked AuNPs by PLAL

1. Introduction

In the last decade, the use of plasmonic systems based on nanoparticles (NPs) has been revolutionizing the analytical spectroscopy, opening the way to extremely high sensitivity with extremely low limits of detection [1]. One of the most recent application of plasmonic system to analytical chemistry is the NP enhanced laser ablation, that has been exploited mainly for improving the performance of Laser Induced Breakdown Spectroscopy (LIBS) [2, 3] and lately also for Laser Ablation Inductively Coupled Plasma Mass Spectrometry (LA-ICP-MS) [4, 5]. NPs enhanced laser ablation is based on the interaction of the plasmonic system of metallic NPs with the ablated matter during the laser pulse irradiation with ns-laser pulse. Although several aspects still need to be elucidated, differently to the Surface Enhanced Raman Scattering (SERS), in the case of NPs enhanced laser ablation, the high energy laser pulse is used for inducing a plasma, initially at density very close to the sample/target material. The concentration of the electromagnetic field of the laser pulse between the NPs, coupling with the high density ablated matter allows to transfer the laser energy to the sample in a much more efficient way with respect to conventional laser ablation [6], allowing the enhancement of the analytical signal up to two orders of magnitude. It was already demonstrated [7, 8] the high efficiency of NP enhanced Laser Induced Breakdown Spectroscopy (NELIBS) with respect to LIBS when analyses are performed on biological systems. Organic samples upon laser irradiation tends to produce weak plasmas because of elements with high ionization energy such as carbon, nitrogen, hydrogen and oxygen, therefore the LIBS trace analysis can be difficult. On the contrary, the use of a layer of NPs where the organic solution is dropped and dried allows a notable increase of the plasma duration and of the emission intensity with consequent improvement of the analytical sensibility.

In this paper a different investigation of NP enhanced laser ablation is proposed. NELIBS is performed in presence of proteins. The plasmonic effect due to NPs surface properties, such as charges, is perturbed by the interaction with proteins and the consequent effect on plasma emission is studied and correlated to the structure of the NP-protein complex. In this view this paper is aimed to prove the concept that NELIBS can be exploited as a sensing tool. The NPs used during these experiments were ultrapure gold NPs (AuNPs), stable without any stabilizer [9], incubated with proteins in order to form the NP-protein complex solution. It is well known that proteins adsorbed on gold NPs allow the formation of the protein corona (PC) on their surface [10] inducing a variation of

the NPs surface properties. Then, after the drying of NP-protein complex solution on the target, NELIBS was performed. Instead of focusing our attention to the improvement of the analytical signal, the effect of the NP- protein interaction is investigated with the observation of how the amount of the adsorbed protein on the NP surface affects the electromagnetic field enhancement of the NPs system during the ablation process. This effect has been investigated with the study of the dependence of the signal enhancement on NP-protein interaction, during NELIBS of a titanium sample. This inverse approach to NELIBS is aimed to demonstrate that NP enhanced laser ablation, although based on high irradiance laser-matter interaction and to breakdown process, is extremely sensitive to the employed colloids, especially if the colloid is covered by organic layers. Therefore, this approach allows the sensing of the structural characteristics of AuNP-protein complexes in terms of ability of NELIBS to detect the protein surface coverage and in turn it opens the way to potentialities beyond the elemental analysis, as for example, the sensing of the protein corona formation. Considering that AuNPs when introduced in a biological medium form the PC immediately, there is a growing interest about the PC sensing in order to exploit its role in influencing the potential applications of AuNPs in biomedicine [11-13]. Moreover, the determination of the surface coverage in PC [14] is an important issue for the quality control of protein-modified nanoparticles surface in different nanotechnology fields as, for example, nanoparticle-based biosensors and protein-enabled nanomaterials for biomarker.

On the other hand, this study can be also addressed to the optimization of biological sample analysis with NELIBS, since it points out how the adsorbed protein content on NPs can affect the LIBS signal enhancement.

In this frame, NELIBS with two different AuNP-protein complexes has been studied. Human Serum Albumin (HSA) and Cytochrome C (CytC), having both strong affinity for the gold surface due to the presence of single free exterior thiol (associated with a cysteine residue) [15], bind to AuNPs forming a long term stable protein corona. Although the addressed test cases appear simpler than a real biological application, at this stage where for the first time such approach is proposed, long term stable protein corona systems allow the investigation of the fundamental aspects of the potential use of NELIBS as a sensing tool. The colloidal solutions have been characterized with Dynamic Light Scattering (DLS), Surface Plasmon Resonance (SPR) spectroscopy and Laser Doppler Electrophoresis (LDE, for ζ-potential determination), and then deposited on a titanium metallic substrate. Transmission Electron Microscopy (TEM) has been finally employed in order to monitor the shape and the structure of AuNPs and AuNP-protein complexes after drying. The Ti-NELIBS emission signal has been then recorded at different protein/NP ratios and normalized with respect to the corresponding emission signal with LIBS. The observation has been then correlated to the colloidal solution properties.

The results show that the dependence of the NELIBS enhancement is strongly correlated to the structure of the NP-protein complex as protein content absorbed on the NPs surface, and in turn it gives specific response on the employed protein depending on the protein size.

2. Scientific background on NELIBS.

Nanoparticle Enhanced Laser Induced Breakdown Spectroscopy is the optical emission signal of laser induced plasma obtained with laser ablation after the deposition of plasmonic NPs on the surface of the sample. The fundamental mechanisms allowing the emission enhancement are reported in previous papers [2, 6]. Briefly, when metallic NPs are deposited on the sample surface, laser

irradiation is more effective as a consequence of the coupling of the electromagnetic field of the laser with the one produced by the plasmonic system. In ref. [6] it has been observed that although the laser irradiance is beyond the breakdown threshold of the sample to form the plasma, the NPs do not vaporize during the laser pulse and allow the electromagnetic field enhancement effect along the all pulse duration and in turn the effective interaction of the plasmonic system with the high density ablated matter in the first stage of expansion. The main characteristics that have been observed are the following:

a) Same amount of removed matter per laser shot than traditional ablation.
b) Higher atomization yield of the ablated matter.
c) Better laser pulse energy distribution on the sample.
d) Multi ignition point for the plasma induction.
e) Enhancement of the plasma emission signal up to two orders of magnitude with respect to conventional LIBS.

The enhancement of the emission spectra with NELIBS, defined as the ratio between emission line intensity of NELIBS and LIBS, is strongly related to the efficiency of the plasmonic coupling between the NPs. This means that 2D deposition with suitable inter-particle distance are required. Generally, the deposition of the NPs is accomplished by depositing and then drying a drop of colloidal solution directly on the sample surface. The concentration of the colloidal solution needs to be optimized in order to achieve a 2D layer of NPs with suitable inter-particle distance [16]. This operation is the most difficult stage of NP enhanced laser ablation, because during the drying of the droplet aggregation and double NPs layer should be avoided in order to maximize the NELIBS effect. Since the NELIBS enhancement of the plasma emission is extremely sensitive to the deposited plasmonic system, in this paper, this is exploited to correlate the enhancement magnitude to the NP-protein complex structure.

3. Materials and methods

3.1 Experimental set-ups

The NELIBS experiments were performed by using an Nd:YAG laser, Quantel Q-smart 850, with a pulse duration of 6 ns operating at 1064 nm with energies up to 615 mJ/pulse. During experiments, the employed laser energies were 360 and 260 mJ with the corresponding laser crater diameters of 1.7 ± 0.1 mm and of 1.5 ± 0.1 mm, respectively in order to obtain similar fluence of 15 J/cm^2. The laser crater was monitored with a digital microscope, Dinolite. The spectrometer used was a Czerny-Turner (JY Triax 550) coupled with an ICCD (JY 3000) which was synchronized with the laser source by a pulse generator (Stanford DG 535) for performing emission spectroscopy of the plasma. The sample, positioned on a micrometric stage, was placed perpendicularly to the laser beam focused with a 50 mm focal length lens. The plasma emission was finally focused directly on the slit of the spectrometer by an objective (N4X-PF - 4X Nikon Plan Fluorite Imaging Objective, 0.13 NA, 17.2 mm WD), The monochromator slit was set to 100 μm and the detector gate width was set at 5 μs with delay of 1 μs. LIBS and NELIBS spectra were acquired by employing one laser shot and four replica were done for each employed colloidal solution. The experiments consist in firing laser pre-shots, the last of which was used to acquire the LIBS signal. After the deposition and drying of the colloidal solution on the formed crater, a further laser shot was fired for NELIBS. Each measurement was performed on a fresh sample surface by moving the sample with a micrometric stage. Fig. S1 shows the NELIBS experimental set-up.

The Vis SPR spectra of both AuNPs and AuNP-protein complexes in the region between 400 and 800 nm were registered using an Agilent 8453 UV–vis diode-array.

AuNPs and AuNP-protein complexes were characterized by DLS and by LDE measurements using a Zetasizer-Nano ZS from Malvern Instruments. All measurements were carried out at 25 °C. DLS measurements were performed in backscattering at a fixed detector angle of 173°. Three measurements were acquired for each sample, and each reading was composed of at least 12 runs. The LDE measurements were performed at the stationary levels of a capillary cell and the scattered light was collected in forward scattering at a fixed detector angle of 17°; the average electrophoretic mobility was retrieved with a fast field reversal (FFR) sequence (high frequency alternating electric field) while the distribution of electrophoretic mobilities has been obtained using slow electric field reversal (SFR) sequence [17]. The ζ-potential was subsequently evaluated from the electrophoretic mobility according to the Hückel approximation. Each sample was measured 3 times and each measurement consisted of a variable number of up to 100 acquisitions.

Transmission electron microscopy (TEM) was performed with an FEI Tecnai *Spirit* 12 (Hillsboro, OR, USA) instrument (high tension: 120 kV; filament: LaB_6), by dropping NP suspensions on a Formvar®-coated Cu grid (300 mesh, Agar Scientific, Stansted, UK). The microscope was calibrated by using the S106 Cross Grating (2160 lines/mm, 3.05 mm) supplied by Agar Scientific. Alignments and astigmatism correction were carried out following factory settings and fast Fourier transform processing, respectively. TEM images processing was performed manually, through the ImageJ® (version: Java 1.8.0_172) free software.

3.2 NELIBS sample preparation

Titanium target (Ti, 99.995% pure, 2.00" diameter x 0.250" thick, ± 0.010" all, K.J. Lesker) was utilized as a sample throughout the whole experiment. The titanium surface was polished with sandy paper, cleaned with soap and rinsed several times with milliQ water in ultrasonic bath. The solutions were deposited on crater induced by 8 cleaning laser pre-shots over the titanium surface in the form of a drop as shown in Fig. S2. The volume of each solution drop was 2 µl. Due to difference in surface hydrophobicity between crater and sample surface, the whole drop was contained, and consequently get dried, inside the pre-shots crater size. The drop was gently dried with airflow. The single laser shot employed for the NELIBS leaded to a complete ablation of the dried drop.

3.3 Gold nanoparticles preparation

The AuNPs have been produced by Pulsed Laser Ablation in Liquid (PLAL) as described in details in Ref. [9]. To produce AuNPs, a gold target (99.999%, Kurt J. Lesker Company) immersed in ultrapure water (Chromasolv^M Plus, Honeywell) with KCl 100 µM was employed. A 8 ns laser, NdYAG (Quanta System PILS-GIANT) with wavelength of 1064 nm, repetition rate of 10 Hz, a fluence of 64 J/cm^2 as well as a plano convex lens of 5 cm focal length for laser focusing were used.

After preparation, the AuNPs have been characterized by means of several techniques and AuNP concentration was evaluated from the visible spectrum of the surface plasmon resonance (SPR) as described in [9].

Before use, AuNPs were suitably diluted with 100 µM KCl or with 5 mM Carbonate buffer, pH= 10.5, depending on the experiment to be performed.

Fig S3a and Fig S4a show respectively the SPR visible spectra of AuNPs in both 100 μM KCl and 5 mM Carbonate buffer, pH= 10.5. A single plasmonic band, centered on 517 nm, denoting well dispersed NPs, is evident. Figs S3b and S4b show TEM images of AuNPs respectively in KCl and in Carbonate buffer, while in Fig S3c and Fig. S4c their distribution sizes obtained from TEM images are reported. In table 1 the AuNPs diameters retrieved from TEM distribution size fitted with a log-normal distribution and from the average of the whole set of measured NPs as well as the hydrodynamic diameter measured with DLS are summarized. For TEM diameter obtained with the LogNormal fitting, the mean is reported with the standard deviation retrieved by the fitting, that takes mainly into account the fitting quality. The ζ-potential values of the AuNPs in both KCl and Carbonate buffer are also reported in table1. The negative ζ-potentials measured in both conditions evidences the high colloidal stability of prepared AuNPs.

Table 1. Sizes (diameters), ζ-potential of AuNPs. The error on diameters and on ζ-potential is the standard deviation. For TEM, the mean from LogNormal fitting and the average of whole set of measured AuNPs with their respective standard deviations are presented.

	Size (diameter) /nm			**ζ-pot / mV**
	DLS	**TEM**		
	D	**$D_{LogNormal}$**	**$D_{Average}$**	
AuNPs in 100 μM KCl	13±2	9.2±0.2	10±3	-57.48±1.5
AuNPs in 5 mM Carbonate buffer (pH=10.5)	14±3	8.7±0.2	10±4	-55.72±2.8

3.4 Proteins and AuNP-protein complex solutions preparation

Two proteins with high affinity for AuNPs surface have been employed, in order to secure the stability of the formed AuNP-protein complexes. The chosen proteins were Human Serum Albumin (HSA,) and Cytochrome C (CytC). HSA consists of 585 aminoacids with a molecular weight of 66.5 kD and presents single free cysteine residue at position 34 (Cys34) [18]. Cytochrome c, is a low molecular mass protein (ca. 12 kDa) containing a heme group, which is covalently bound to two cysteines of the amino acid sequence. In this work we use the Yeast iso-1-cytochrome c isolated from *Saccharomyces cerevisiae* (YCc), that presents a free cysteine in position 102 (Cys102). In principle, the interaction with NPs could induce changes in the conformation of proteins, affecting their functionality and allowing the formation of complexes in which their nature is altered. In this respect, it has been demonstrated that both proteins HSA and YCc, after the interaction with the spherical AuNPs, undergo only to minor conformational changes in α-helical [19, 20], which makes these proteins suitable for forming stable AuNP- protein complexes.

HSA (purchased from Sigma-Aldrich, cod A3782, CAS Number: 70024-90-7) was solubilized in 100 μM KCl. HSA-AuNP complexes were prepared by mixing an AuNP solution (as prepared in 100 μM KCl) with an appropriate amount of a HSA solution to obtain the desired [HSA]/[AuNP] ratio. In the case of HSA the final AuNP concentration was fixed to 10.5 nM or to 28.5 nM. The prepared mixtures were kept at 25°C for 24h before measurements, in order to reach the equilibrium in the solution.

Cytochrome C from *Saccharomyces cerevisiae* (purchased from Sigma-Aldrich, cod C2436, CAS Number: 9007-43-6) was solubilized in 5 mM Carbonate buffer, pH= 10.5. Cyt C-AuNP complexes were prepared by mixing of an AuNPs solution (with pH adjusted to 10.5 by a proper addition of Carbonate buffer) with an appropriate amount of a Cyt C solution to obtain the desired [Cyt C]/[AuNP] ratio, keeping fixed the final AuNP concentration to 10.5 nM. Solution were kept at 25°C for 24h before measurements for reaching the equilibrium.

It should be noted that the Cyt C-AuNP complexes were prepared at pH 10.5, a value to which they are well dispersed in solution and avoid aggregation. AuNPs produced by PLAL are stable in solutions in a range of pH between 4 and 11 [21], but in presence of CytC the stability of the formed complexes has a strong dependence from the solution pH. Ref. [20] demonstrated that Cyt C-AuNP complexes (prepared with YCc) are stable at pH higher than 10, while at pH below 10 aggregation occurs. Our experiments, performed at pH= 10.5 and 7.0, confirmed this behaviour (see Fig. S5a for details). Based on these considerations, in present work the AuNP- CytC complexes have been prepared in Carbonate buffer at pH 10.5.

After preparation, AuNP- protein complexes have been characterized by TEM in order to control the shape and size of AuNPs after their interaction with proteins (Fig.S6, S7). The presence of proteins does not induce any alterations on AuNPs size distribution.

4. Results and discussion

4.1 NP- protein corona complex characterization

The protein corona formation is a dynamic process depending on the binding affinity and rate of absorbed protein on NPs. Proteins, depending on their composition, size, surface charge, can adsorb and desorb to the surface of NPs. The equilibrium between the free proteins in solution and the bound proteins on the surface is reached when the absorption and desorption rates of proteins become equal and the continued exchange will not affect the composition of the corona [22]. A long term [15] high affinity binding of proteins on NPs forms the so called “hard” corona consisting in bound proteins that do not readily desorb from the surface and that can covalently bound the NPs surface. The number of proteins needed for the corona formation depends on the size of both NPs and proteins.

In this paper, the two employed proteins, for the AuNP- protein complexes, HSA and CytC, have both a free cysteine residue and have an extremely different size. They are therefore chosen for the NELIBS measurements not only for their strong and similar affinity for the gold surface but also because at fixed AuNPs concentration a markedly different number of proteins to form a layer of protein on NPs is needed.

To have an estimation of the concentration of HSA and CytC needed to form a single protein corona, the number of proteins required has been estimated theoretically. The number of protein binding sites on NPs surface depends strictly on the NPs and protein sizes. An ideal maximum number of proteins adsorbed on the NPs surface can be retrieved by considering, in first approximation, the proteins as spheres physically in contact with the nanoparticle surface. Therefore the ratio between the NPs surface and the cross-section of the proteins gives a geometrical prediction [14] on the maximum number of binding sites:

$$N_{geo} = \frac{4\pi {R_{AuNPs}}^2}{\pi {R_g}^2}$$ Eq. 1

Where R_{AuNPs} is the NPs radius and R_g is the protein radius of gyration calculated from the protein structure. For the geometrical calculation, the protein radius of gyration is chosen because of the approximation of protein shape to a sphere while for the NPs radius, the hydrodynamic radius of AuNPs measured with DLS has been used, since the calculation refers to a protein corona formed in the solution. The determination of the number of binding sites on NPs is a more complex issue with respect to a simple geometrical prediction, since it depends on some variables as the real geometry of the protein (usually globular), the NPs surface reactivity, the protein-protein interaction, and so on. In any case, for the main aim of this paper, this last issue is out of scope and the geometrical calculation can give a fast indicative prediction on the concentration of the employed proteins needed to form a single layer of protein corona. Once N_{geo} is known, the concentration of proteins needed to form a single layer of proteins corona can be easily determined:

$$[protein]_{geo}^{corona} = N_{geo} \cdot [AuNPs]$$ Eq. 2

Where [protein] and [AuNPs] are the molar concentrations of protein and AuNPs, respectively.

The parameters (R_g) taken from literature and employed for the geometrical calculation of the concentration of proteins needed for the formation of a single layer of proteins corona are shown in Table 2, which also reports the N_{geo} calculated for both proteins and the relative concentrations needed to form a single layer of PC.

Table 2 AuNP size and concentrations, protein gyration radii from literature, geometrical prediction of protein unities and protein concentrations.

	[AuNPs] (nM)	R_{AuNPs}^{DLS} (nm)	R_g^{HSA} (nm) [18]	R_g^{CytC} (nm) [23]	N_{geo}^{HSA}	N_{geo}^{CytC}	$[HSA]_{geo}^{corona}$ (μM)	$[CytC]_{geo}^{corona}$ (μM)
1st case	10.5	6.5	2.6	1.39	25	87	0.26	0.92
2nd case	28.5	6.5	2.6	1.39	25	87	0.71	-

SPR spectroscopy and DLS have been used to monitor the formation of protein corona [24-25] and its stability as function of time.

Fig. 1a shows the absorbance spectra of bare AuNPs and AuNP-protein complexes formed in presence of the protein concentration at which the corona is obtained ([HSA]= 0.25 μM and [CytC]= 0.9 μM, see table 2).

The prepared AuNPs have the peak of the plasmon resonance band at 517 nm. By the inspection of figure it can be observed, for both complexes, a red shift of the wavelength at the maximum of absorbance with respect to the one of bare AuNPs. This shift is due to the variation of the refractive index of the NPs surrounding and is an evidence of the presence of a protein layer [25].

SPR has been used also to follow the stability of both types of complexes over time. For what concerns the AuNP-HSA complex, FigS5b shows the trend of the red shift of the wavelength at the

maximum of absorbance ($\Delta\lambda_{max}$= $\lambda_{max\text{-}AuNPs+HSA}$-$\lambda_{max\text{-}AuNPs}$) as function of time after the HSA incubation. It is clearly evident that after a few minutes $\Delta\lambda_{max}$ reaches a maximum value and it remains constant for a long time. The inset of Fig. S5a shows the stability of the Cyt C-AuNP complex at pH 10.5 over time. These experiments demonstrate both the formation of the AuNP-protein complexes and their stability in time.

Fig.1b shows the corresponding size distributions of the as prepared AuNPs, and AuNP-protein complexes estimated with DLS measurements. As it can be observed, at [HSA]= 0.25 μM and at [CytC]= 0.9 μM, an increase of average diameter for both complexes is visible and it can be ascribed to the protein corona formation. An increase of average diameter from 13±2 nm (measured for free AuNPs) to 21±2 nm for AuNP- HSA complex and to 18±2 nm for AuNP- Cyt C complex, is respectively observed. The observed increase of the diameter is reasonable if we take into account the measured hydrodynamic diameters of HSA, 5.24±0.08 nm, and of CytC, 3.2± 0.3 nm, which are also closely similar to the gyration diameters reported in table 2. So, the measured sizes of NP- protein complexes are indeed comparable to the sizes obtained on the basis of $D_{AuNP\text{-}protein}$ shown in the inset of Fig. 1b, which are about 23 nm and 19 nm for AuNP-HSA and AuNP- Cyt C, respectively.

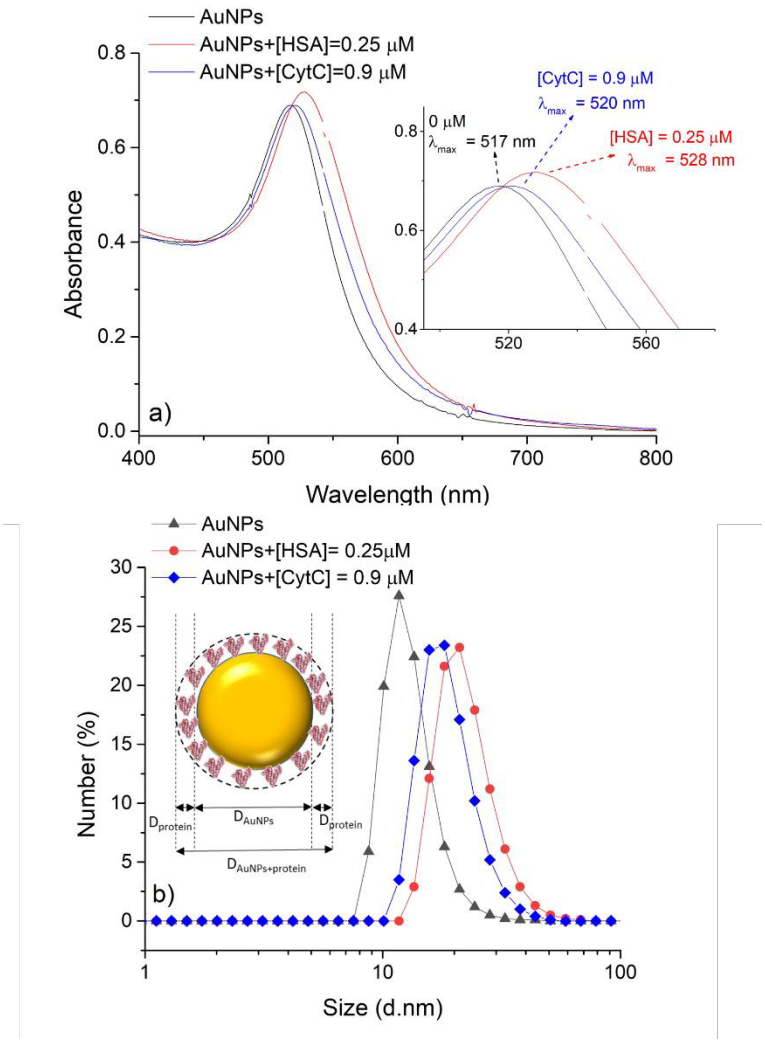

Fig. 1 a) Absorbance spectra of AuNPs, AuNP-HSA and AuNP- Cyt C complex solutions. Inset reports an enlargement of the spectra in the maximum absorption region. b) DLS hydrodynamic size distributions of AuNPs, AuNP-HSA and

AuNP- Cyt C complexes. The inset shows the conceptual model for the geometrical calculation of the complex diameter. ([HSA] =0.25 μM, [CytC] = 0.9 μM).

4.2 Effect of NP- protein complex on NELIBS enhancement.

Solutions of AuNP- protein complexes obtained at fixed concentration of AuNPs incubated with increasing concentration of protein have been employed for NELIBS experiments, in order to investigate their effect on the enhancement of Ti-substrate emission lines as function of protein concentration. SPR (data not shown), DLS and ζ-potential was systematically applied to each colloidal solution employed for the NELIBS measurements. Since the solution was dried on metallic sample to perform NELIBS, also TEM measurements of AuNPs with different concentration of proteins have been performed, to control the shape and structure of the AuNPs after drying.

A frame of the emission spectra of titanium of LIBS and NELIBS with AuNPs and AuNPs with protein is reported in Fig.2 in order to show the improvement of NELIBS intensity with respect to LIBS. All the emission lines in this portion of the plasma emission spectrum belong to Ti I electronic transition. By the inspection of Fig.2 it can be noted that NELIBS has higher emission intensity with respect to LIBS and that the concentration of protein in the colloidal solution affects the intensity of NELIBS spectra. In the following, it will be reported the enhancement as the line intensity ratio of Ti I at 462.31 nm obtained with NELIBS and LIBS. The intensity of an emission line is extracted by the peak area with a Voigt fitting process [26].

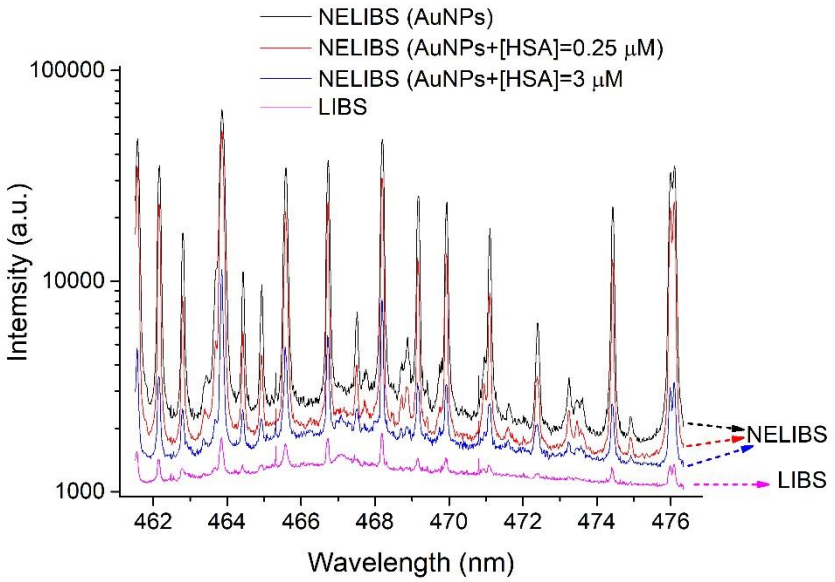

Fig. 2 Emission spectra during LIBS and NELIBS of Ti target with AuNPs and with AuNPs+HSA at two HSA concentrations, 0.25 μM and 3 μM, respectively. (E_{laser}= 360 mJ, laser spot size = 1.7 ± 0.1 mm).

The first NELIBS experiments were performed in presence of HSA. Two different sets of samples were prepared, each containing a fixed concentration of AuNPs (namely 10.5 nM or 28.5 nM) and varying concentrations of protein. Different concentrations of AuNPs require different concentration of proteins to form a single layer of proteins corona, as reported in Table 2, where calculated values are shown.

Fig. 3 shows that the trend of NELIBS enhancement varies as function of the added HSA, for both AuNPs concentrations. The maximum enhancement is obtained at HSA concentrations close to that calculated to form the corona: i.e. $[HSA]_{geo}^{corona}$ = 0.26 μM for 10.5 nM AuNPs and $[HSA]_{geo}^{corona}$= 0.71 μM for 28.5 nM AuNPs.

By plotting the enhancement as function of number of HSA units in Fig.4a it can be observed that the two maxima of enhancement are coincident, determining an experimental number of HSA needed to form the corona, that is $N_{exp}^{HSA} = 28 \pm 4$, in good agreement with $N_{geo}^{HSA} = 25$.

ζ-potential measurements have been performed to monitor the surface charge of the AuNP-HSA complex when different concentrations of protein are added to the bare NPs.

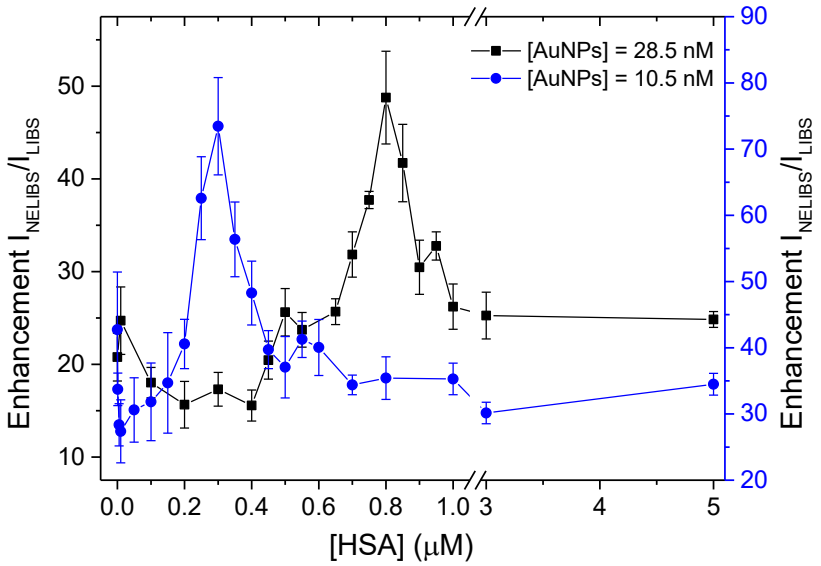

Fig.3 NELIBS enhancement as function of HSA concentration at two fixed AuNP concentrations: 10.5 nM and 28.5 nM. (E_{laser}= 260 mJ, laser crater diameter = 1.5 ± 0.1 mm)

AuNPs alone in solution present a ζ-potential of about -57 mV (see Table 1). Fig.4b reports ζ-potential values measured at different HSA/AuNPs ratios and shows as the protein absorption on the NPs surface determines a significant reduction of the overall surface charge of the NP- protein complexes, for both AuNPs concentrations tested. As the protein number increases, the ζ-potential of the complexes becomes less negative and it reaches a specific value at the protein number at which corona formation occurs. After the corona formation, the ζ-potential holds a constant value, meaning that no other changes occur on the AuNPs surface.

Also the two ζ-potential curves as function of number of HSA, fitted with similar Hill equation (Langmuir adsorption isotherm) [27, 28] , demonstrate the formation of single corona for the AuNPs size of 13 nm above $N_{geo}^{HSA} = 25$. In the supporting information, more details on the fitting parameters can be found.

The dependence of the NELIBS enhancement on protein concentration shown in Fig 3 reveals important informations.

At very low HSA concentrations a decreasing of the enhancement is observed, after which the maximum enhancement is detected in correspondence of the corona formation. At even higher protein concentrations, the enhancement decreases again. This phenomenon, observed for both AuNPs concentrations, could be related to different types of AuNPs deposition on the titanium substrate, obtained during sample drying, for different HSA concentrations.

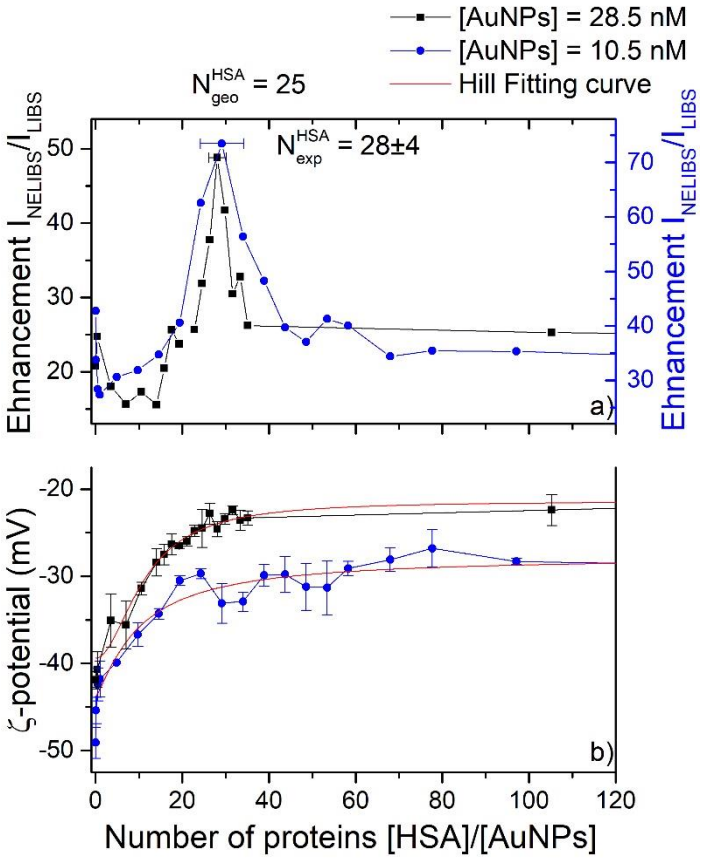

Fig. 4 a) NELIBS enhancement and **b)** ζ-potential data reported as a function of number of HSA added at two fixed AuNP concentrations: 10.5 nM and 28.5 nM. (E_{laser}= 260 mJ, laser crater diameter = 1.5 ± 0.1 mm). Red lines represent fits to Langmuir adsorption isotherms. Fitting parameters are reported in SI.

At protein concentrations below the one that allows the corona formation, the increase of the ζ-potential values measured for AuNP-protein complexes (see Fig. 4) denotes a partial neutralization of the NP surface charges, due to the bounded proteins, that can induce NPs aggregation. As a result of this, during the droplet drying on the substrate surface, large clusters with random three dimenional shape can be deposited. This is observable in the TEM image shown in Fig.5, for 0.1 μM HSA. If NPs are not deposited in a single layer, defect on plasmon system induces tunnelling effect and degradation of the plasmon resonance and consequently the NELIBS signal decreases.

The situation becomes different when the proteins concentration is in the range of concentration where corona formation occurs. Although the ζ-potential shows an even less negative value than the previous scenario, each NPs is surrounded by the protein shell preventing the massive aggregation of the NPs, also during the drying stage. As shown in the corresponding TEM images (at 0.25 μM HSA),

after drying the colloidal solution, clusters of NPs well distributed in bi-dimensional layers are observable on the substrate surface. This NPs distribution allows an optimized coupling of the plasmonic system. In this view, the enhancement reaches a maximum when the protein corona is completely formed.

When the HSA concentration exceeds the number of proteins needed to form the corona, the enhancement begins to decrease. The drying of the solution containing an excess of proteins can affect the organization of AuNPs on the sample surface as proteins can fill the interspace between NPs. Thus, NPs precipitate quite far from each other and their plasmonic coupling is weakened. At very high HSA concentration, the enhancement becomes lower since the AuNPs dried on titanium are completely immersed in the protein matrix that reduces further the signal introducing the classical effect of the organic matter on plasma formation. This effect is visible in Fig. 5 where TEM image acquired at 1 µM HSA (excess of proteins in solution) clearly shows the presence of organic material around the AuNPs.

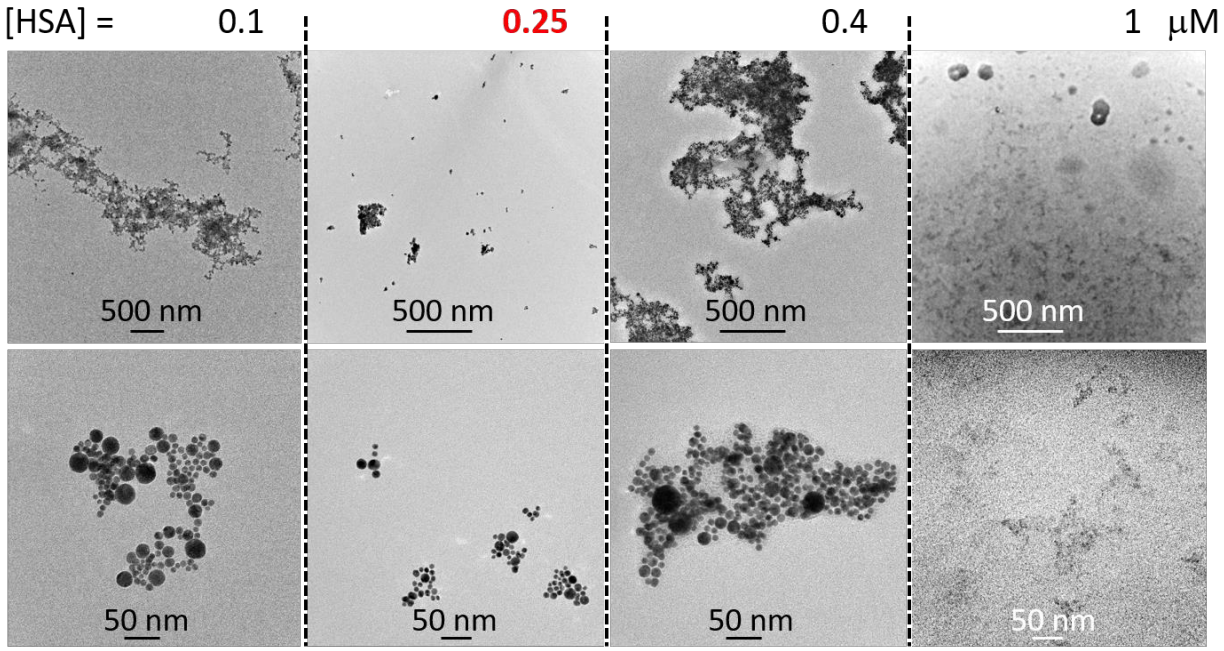

Fig.5 TEM images of the AuNP-HSA complex at four HSA concentrations, 0.1, 0.25 , 0.4 and 1 µM, respectively. The two rows of the figure present two different magnifications of the same sample.

A second set of NELIBS experiments was performed on AuNP- CytC complexes, prepared at fixed concentration of AuNPs (10.5 nM) and varying CytC concentrations.
In the following, obtained results will be shown in comparison with those obtained for HSA in the same conditions of AuNPs and protein concentration.
Fig. S8 shows the comparison of the obtained NELIBS enhancement as a function of the concentration of both proteins. Also in the case of CytC the enhancement reaches its maximum at a concentration very close to that calculated to form the corona: i.e. 0.92 µM. Fig. 6a summarizes NELIBS enhancement results obtained for both proteins as function of number of proteins. It can be observed that the maxima of enhancement is obtained for 86.5 CytC units, allowing the experimental determination of protein number needed to form the corona, in good agreement with the calculated one ($N_{geo}^{CytC} = 87$). The CytC protein number needed to form the corona results to be higher than that required for HSA, due to their different size.

Fig. 6 also shows the corresponding DLS and ζ-potential data obtained for each solution employed for NELIBS.

Fig.6b reports size values measured at different protein/AuNP ratios for both HSA and CytC. The protein absorption on the NPs surface determines a significant increase of the size, reaching a plateau at around 23 nm and 18 nm for AuNP-HSA and AuNP-CytC complexes, respectively.

The trend of the complex sizes reveals that the values of the plateaux corresponds to the geometrical sizes that the complexes should have when a single layer of protein corona is formed. The variation of the hydrodynamic radius of the NP- protein complexes as function of the number of the added proteins indicates that, when the proteins begin to be adsorbed on the NPs surface, the size of the NPs increases until the binding absorption sites on the NPs surface are saturated. If the coverage of proteins on the NPs surface corresponds to a monolayer of proteins, the hydrodynamic radius holds a constant value even if an excess of proteins is added with respect to the number of proteins needed for the protein corona formation [27].

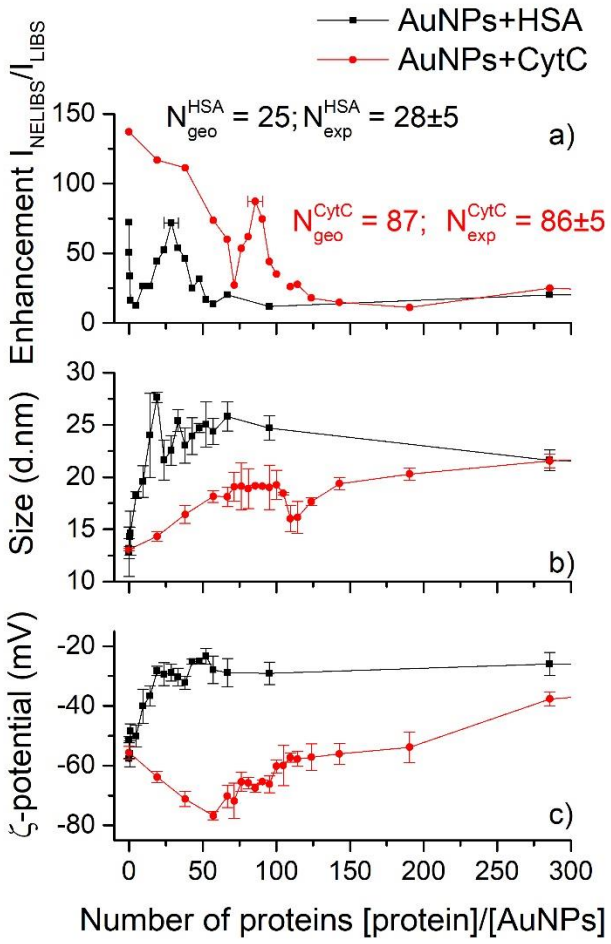

Fig.6 a) NELIBS enhancement, **b)** hydrodynamic diameter and **c)** ζ-potential data reported as a function of number of proteins (HSA and CytC) added at 10.5 nM AuNPs concentrations. (E_{laser}= 360 mJ, laser crater diameter = 1.7 ± 0.1 mm)

The trend of ζ-potential as function of number of added proteins, also shows the formation of protein corona (as previously described) for both complexes (Fig. 6c). In the case of AuNP-CytC complex, when the protein concentration is very low, it can be noted an initial decreasing of ζ-potential –in terms of negative value) and, only after a certain concentration, the ζ-potential increases again for

reaching a plateaux. This behaviour is due to the presence of the carbonate in this colloidal solution and the consequent interference between carbonate and protein with the AuNPs: only after a certain number of protein occupies the NPs surface binding sites, the surface charge of the NPs begins to decrease because of the interaction of AuNPs and the protein. Overall, the size and ζ-potential data reported as function of number of proteins clearly indicate the protein corona formation in solution around a number of added proteins of N_{geo}^{HSA}= 25 and N_{geo}^{CytC} = 87 for HSA and CytC, respectively. These values are in very good agreement with the ones experimentally found with the NELIBS, N_{exp}^{HSA}= 28±4 and N_{exp}^{CytC} = 86±5 for HSA and CytC, respectively.

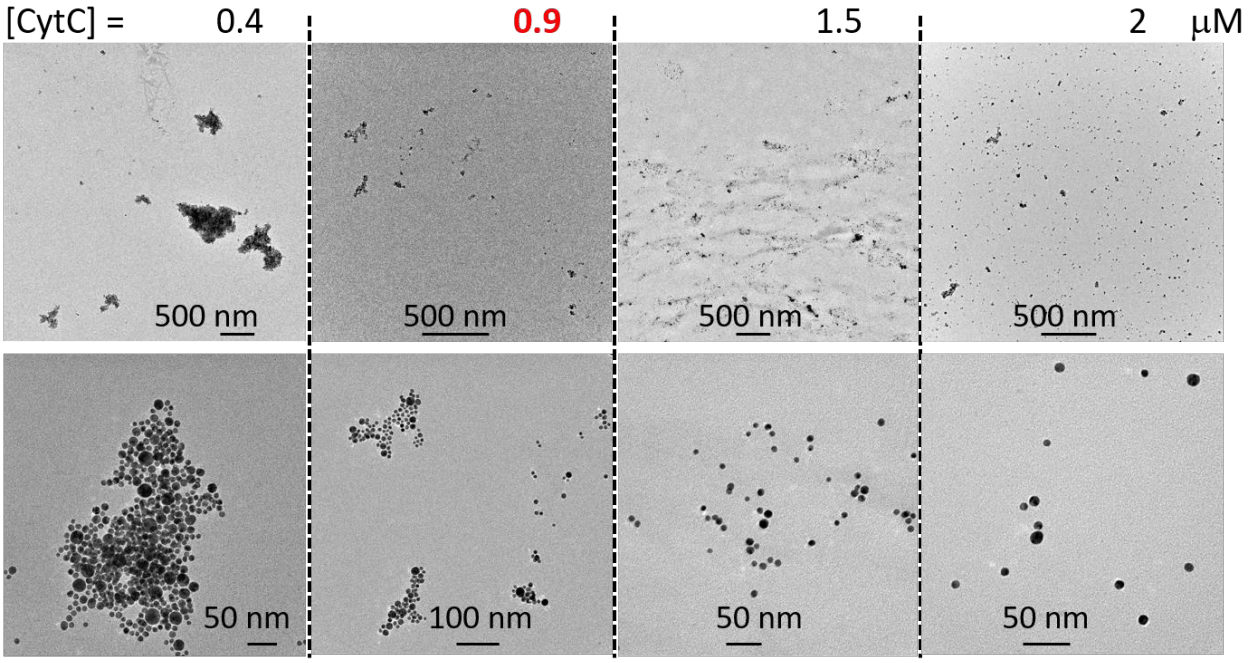

Fig. 7 TEM images of the AuNP-CytC complex at four HSA concentrations, 0.4, 0.9 , 1.5 and 2 μM, respectively. The two rows of the figure present two different magnifications of the same sample.

As already seen for HSA test case, the dependence of NELIBS enhancement on CytC concentration shown in Fig S8 could be related to different types of AuNPs deposition on the titanium substrate, obtained during sample drying. At protein concentrations lower than that one allowing the corona formation, during the droplet drying on the substrate surface, NPs aggregation occurs. This is shown by TEM images in Fig. 7, for 0.4 μM CytC, where three-dimensional NPs clusters are evident, in agreement with the decrease of NELIBS signal registered. At protein concentrations at which corona formation occurs, after drying, NPs are well distributed in bi-dimensional layers on the substrate surface, as shown in Fig. 7 for 0.9 μM CytC. In this condition, a good coupling of the plasmonic system is obtained, allowing the maximum of enhancement. At high CytC concentration, the presence of an excess of proteins generates dried AuNPs immersed in the organic matrix and far from each other, as evidenced by TEM images for 1.5 and 2 μM CytC. In these conditions, the NPs plasmonic coupling is weakened and the enhancement decreases.

In order to investigate the effect of the plasmonic system arrangement on the surface, the interparticle distance has been estimated as $d_{INT} = D_{c-c} - d$ [29], where D_{C-C} is the centre-to-centre distance between two adjacent AuNP-protein complexes whose value is statistically measured from

logNormal distribution of several D_{CC} measured from TEM images; d is the AuNPs diameter obtained from logNormal distribution of NP diameters measured from TEM images (table 1). The distance of the deposited NPs on the sample surface is reported in Fig.8. The Fig.8 shows that the distance increases at protein concentration higher than the one of the corona. As the increase of the inter-particle distance implies the decreasing of the effective plasmonic electromagnetic field, NELIBS signal decreases. It is interesting that when the corona is formed the absolute value of the enhancement (see Fig.6) is the same within the experimental error as well as the inter-particle distance for both the investigated NP- protein systems, denoting that the typology of protein does not affect notably the enhancement when optimal conditions are reached, because the enhancement of the electromagnetic field, as well as the NELIBS one, mainly depends on the NPs plasmon resonance. On the contrary, as mentioned above, the decreasing of the signal for low protein concentration is due to the formation of aggregate during the drying process. In this case, the effect of the smaller inter-particle distances is mitigated by the three-dimentional cluster deposited on the surface that decreases the efficiency of the electromagnetic field on the sample surface.

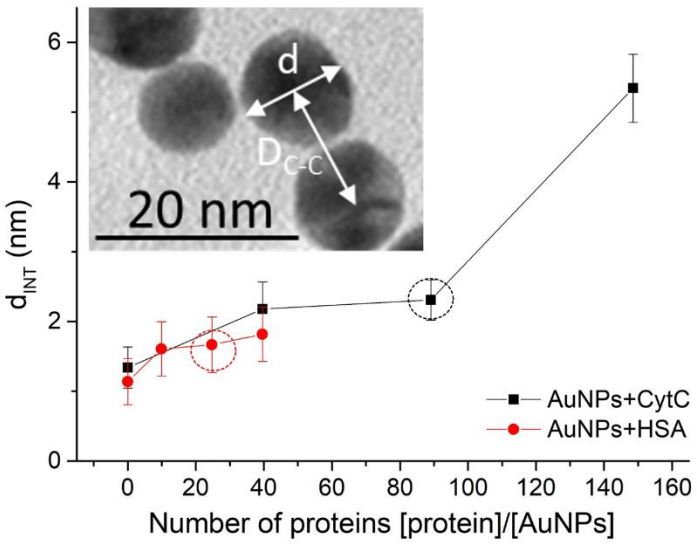

Fig.8 AuNPs interparticle distances ($d_{INT} = D_{c-c} - d$) as function of number of added proteins (HSA, CytC), estimated from TEM images of AuNP-protein complexes.

5. Conclusions

In this paper NP-protein system mediated NELIBS has been investigated in order to search a correlation between NELIBS enhancement and the structure of the NP- protein complexes. Although LIBS is based on the sample breakdown and atomic plasma induction, the use of NPs for improving the signal has been demonstrated to be very sensitive to the plasmonic interactions with the incoming laser beam. Two different NP- protein systems have been studied and they are HSA and CytC, having both strong affinity for the AuNPs due to the bonding between the single free exterior thiol and gold surface but quite different size. With the present experiment, it has been observed that the Ti-NELIBS enhancement strictly depends by the NP- protein structure and on the plasmonic organization reached after the NP deposition process on the sample. Several techniques including DLS, SPR, ζ-potential and TEM, have been employed for the characterization of the NP-protein complex solution and

consequent observations have been correlated to the NELIBS enhancement as function of the NPs/protein concentration ratio. Finally, the NELIBS maximum of enhancement allowed measuring the number of protein units that form the protein corona. This paper for the first time shows a different use of a laser ablation technique in analytical chemistry that is not the elemental analysis, but the sensing of the number of protein in the AuNP-protein corona system.

Acknowledgements:

The authors would like to thank Prof. Gerardo Palazzo for fruitful discussions and Miss Elena Vaníčková for the collaboration during the experiments.

References:

[1]. Jan Krajczewski, Karol Kołąt taj and Andrzej Kudelski, Plasmonic nanoparticles in chemical analysis, RSC Adv., 2017, 7, 17559

[2]. Dell'Aglio, M., Alrifai, R., De Giacomo, A., Nanoparticle Enhanced Laser Induced Breakdown Spectroscopy (NELIBS), a first review (2018) Spectrochimica Acta - Part B Atomic Spectroscopy, 148, pp. 105-112.

[3]. Koral, C., Dell'Aglio, M., Gaudiuso, R., Alrifai, R., Torelli, M., De Giacomo, A., Nanoparticle-Enhanced Laser Induced Breakdown Spectroscopy for the noninvasive analysis of transparent samples and gemstones, (2018) Talanta, 182, pp. 253-258.

[4]. M. Holá, Z. Salajková, A. Hrdlička, P. Pořízka, K. Novotný, L. Čelko, P. Šperka, D. J. Novotný, P. Modlitbová, V. Kanický, J. Kaiser, Feasibility of Nanoparticle-Enhanced Laser Ablation Inductively Coupled Plasma Mass Spectrometry, Anal. Chem. 90 (20) (2018) 11820-11826

[5]. Annarosa Mangone, Fabrizio Mastrorocco, Lorena Carla Giannossa, Roberto Comparelli, Marcella Dell'Aglio, Alessandro De Giacomo, Nanoparticle enhanced laser ablation inductively coupled plasma mass spectrometry, Spectrochimica Acta Part B 163 (2020) 105731

[6]. Alessandro De Giacomo, Rim Alrifai, Vincent Gardette, Zita Salajková, Marcella Dell'Aglio, Nanoparticle enhanced laser ablation and consequent effects on laser induced plasma optical emission, Spectrochimica Acta Part B: Atomic Spectroscopy, Volume 166, April 2020, 105794

[7]. Dell'Aglio, M.; Salajková, Z.; Mallardi, A.; Mezzenga, R.; van't Hag, L.; Cioffi, N.; Palazzo, G.; De Giacomo, A. Application of gold nanoparticles embedded in the amyloids fibrils as enhancers in the laser induced breakdown spectroscopy for the metal quantification in microdroplets. Spectrochim. Acta - Part B At. Spectrosc. 2019, 155, 115–122

[8]. T. Ohta, M. Ito, T. Kotani, T. Hattori, Emission Enhancement of Laser-Induced, Breakdown Spectroscopy By Localized Surface Plasmon Resonance for Analyzing, Plant Nutrients, Applied Spectroscopy, vol. 63, (2009) Number 5.

[9]. M. Dell'Aglio, V. Mangini, G. Valenza, O. De Pascale, A. De Stradis, G. Natile, F. Arnesano, A. De Giacomo, Silver and gold nanoparticles produced by pulsed laser ablation in liquid to investigate their interaction with Ubiquitin, Applied Surface Science, ,2016, Volume 374, Pages 297-304

[10]. Rana S, Yeh YC, Rotello VM (2010) Engineering the nanoparticle-protein interface: Applications and possibilities. Curr. Opin. Chem. Biol. 14:828–834

[11]. Mahmoudi, M.; Lynch, I.; Ejtehadi, M. R.; Monopoli, M. P.; Bombelli, F. B.; Laurent, S. Protein–Nanoparticle Interactions: Opportunities and Challenges. Chem. Rev. 2011, 111, 5610– 5637, DOI: 10.1021/cr100440

[12]. Masoud Rahman, Sophie Laurent, Nancy Tawil, L'Hocine Yahia, Morteza Mahmoudi, Protein-Nanoparticle Interactions. The Bio-Nano Interface, Springer series in biophysics, 2013, Volume 15, ISBN : 978-3-642-37554-5

[13]. Jingying Liu, Qiang Peng, Protein-gold nanoparticle interactions and their possible impact on biomedical applications, Acta Biomaterialia, Volume 55, 2017, Pages 13-27, ISSN 1742-7061, https://doi.org/10.1016/j.actbio.2017.03.055.

[14]. Siyao Liu, Jeannie Horak, Markus Holdrich, Michael Lammerhofer, Accurate and reliable quantification of the protein surface coverage on protein-functionalized nanoparticles, Analytica Chimica Acta 989 (2017) 29-37

[15]. Kumudu Siriwardana, Ailin Wang,†Karthikeshwar Vangala, Nicholas Fitzkee, and Dongmao Zhang, Probing the Effects of Cysteine Residues on Protein Adsorption onto Gold Nanoparticles Using Wild-Type and Mutated GB3 Proteins, Langmuir 2013, 29, 10990−10996

[16]. Huang, Y., Ma, L., Hou, M., Li, J., Xie, Z., Zhang, Z. Hybridized plasmon modes and near-field enhancement of metallic nanoparticle-dimer on a mirror (2016) Scientific Reports, 6, art. no. 30011

[17]. H. Mateos, A. Valentini, E. Robles, A. Brooker, N. Cioffi, G. Palazzo, Measurement of the zeta-potential of solid surfaces through laser Doppler electrophoresis of colloid tracer in a dip-cell: survey of the effect of ionic strength, pH, tracer chemical nature and size, Colloids Surf. A 576 (2019) 82–90, https://doi.org/10.1016/j.colsurfa.2019.05.006.

[18]. Olivieri JR, Craievich AF. The subdomain structure of human serum albumin in solution under different pH conditions studied by small angle X-ray scattering. Eur Biophys J. 1995;24(2):77-84. doi: 10.1007/BF00211402. PMID: 8582321.

[19]. Tsai, D. H.; DelRio, F. W.; Keene, A. M.; Tyner, K. M.; MacCuspie, R. I.; Cho, T. J.; Zachariah, M. R.; Hackley, V. A. Adsorption and conformation of serum albumin protein on gold nanoparticles investigated using dimensional measurements and in situ spectroscopic methods. Langmuir 2011, 27, 2464– 2477, DOI: 10.1021/la104124d

[20]. Gomes, I., Santos, N. C., Oliveira, L. M. A., Quintas, A., Eaton, P., Pereira, E., and Franco, R. (2008) Probing Surface Properties of Cytochrome c at Au Bionanoconjugates J. Phys. Chem. C 112, 16340– 16347 DOI: 10.1021/jp804766v

[21]. Palazzo G, Valenza G, Dell'Aglio M, De Giacomo A (2017) On the stability of gold nanoparticles synthesized by laser ablation in liquids. J Colloid Interface Sci 489:47–56

[22]. Dell'Orco D, Lundqvist M, Oslakovic C, Cedervall T, Linse S (2010) Modeling the Time Evolution of the Nanoparticle-Protein Corona in a Body Fluid. PLoSONE 5(6): e10949. doi:10.1371/journal.pone.0010949

[23]. Shuji Akiyama, Satoshi Takahashi, Tetsunari Kimura, Koichiro Ishimori, Isao Morishima, Yukihiro Nishikawa, and Tetsuro Fujisawa, Conformational landscape of cytochrome c

folding, studied by microsecond-resolved small-angle x-ray scattering, PNAS, 2002, 99 (3) 1329-1334

[24]. Carrillo-Carrion, C., Carril, M., and Parak, W. J. (2017). Techniques for the experimental investigation of the protein corona. Curr. Opin. Biotechnol. 46, 106–113. doi: 10.1016/j.copbio.2017.02.009

[25]. Michele Vitali, Eudald Casals, Francesc Canals, Nuria Colomé and Victor Puntes, Simple spectroscopic determination of the hard protein corona composition in AuNPs: albumin at 75%, Nanoscale, 2020, 12, 15832

[26]. Motto-Ros, V., Moncayo, S., Trichard, F., Pelascini, F., Investigation of signal extraction in the frame of LIBS imaging, Spectrochimica Acta - Part B Atomic Spectroscopy, 155, 2019, 127-133

[27]. Ricardo Franco and Eulalia Pereira, "Gold Nanoparticles and Proteins, Interaction" in V.N. Uversky et al. (eds.), Encyclopedia of Metalloproteins, DOI 10.1007/978-1-4614-1533-6, Springer Science+Business Media New York, 2013, p.908-915

[28]. Pablo del Pino, Beatriz Pelaz, Qian Zhang, Pauline Maffre, G. Ulrich Nienhaus and Wolfgang J. Parak, Protein corona formation around nanoparticles –from the past to the future, Mater. Horiz., 2014, 1, 301

[29]. Guang Yang, Jagjit Nanda, Boya Wang, Gang Chen, and Daniel T. Hallinan, Jr, Self-Assembly of Large Gold Nanoparticles for Surface-Enhanced Raman Spectroscopy, ACS Appl. Mater. Interfaces 2017, 9, 13457−13470

Table and figure Captions:

Table 1. Sizes (diameters), ζ-potential of AuNPs. The error on diameters and on ζ-potential is the standard deviation. For TEM the mean from LogNormal fitting and the average of whole set of measured AuNPs with their respective standard deviations are presented.

Table 2 AuNPs size and concentrations, protein gyration radii from literature, geometrical prediction of protein unities and protein concentrations.

Fig. 1 a) Absorbance spectra of AuNPs, AuNP-HSA and AuNP- Cyt C complex solutions. Inset reports an enlargement of the spectra in the maximum absorption region. b) DLS hydrodynamic size distributions of AuNPs, AuNP-HSA and AuNP- Cyt C complexes. ([HSA] =0.25 μM, [CytC] = 0.9 μM). The inset shows the conceptual model for the geometrical calculation of the complex diameter.

Fig. 2 Emission spectra during LIBS and NELIBS of Ti target with AuNPs and with AuNPs+HSA at two HSA concentrations, 0.25 μM and 3 μM, respectively. (E_{laser}= 360 mJ, laser crater diameter = 1.7 ± 0.1 mm).

Fig. 3 NELIBS enhancement as function of HSA concentration at two fixed AuNP concentrations: 10.5 nM and 28.5 nM. (E_{laser}= 260 mJ, laser spot size = 1.5 ± 0.1 mm)

Fig. 4 a) NELIBS enhancement and **b)** ζ-potential data reported as a function of number of HSA added at two fixed AuNP concentrations: 10.5 nM and 28.5 nM. (E_{laser}= 260 mJ, laser crater diameter = 1.5 ± 0.1 mm). Red lines represent fits to Langmuir adsorption isotherms. Fitting parameters are reported in SI.

Fig.5 TEM images of the AuNP-HSA complex at four HSA concentrations, 0.1, 0.25 , 0.4 and 1 μM, respectively. The two rows of the figure present two different magnifications of the same sample.

Fig.6 a) NELIBS enhancement, **b)** hydrodynamic diameter and **c)** ζ-potential data reported as a function of number of proteins (HSA and CytC) added at 10.5 nM AuNPs concentrations. (E_{laser}= 360 mJ, laser crater diameter = 1.7 ± 0.1 mm)

Fig. 7 TEM images of the AuNP-CytC complex at four HSA concentrations, 0.4, 0.9 , 1.5 and 2 μM, respectively. The two rows of the figure present two different magnifications of the same sample.

Fig.8 AuNPs interparticle distances ($d_{INT} = D_{c-c} - d$) as function of number of added proteins (HSA, CytC), estimated from TEM images of AuNP-protein complexes.

Figure

Click here to access/download;Figure;Fig.1.tif

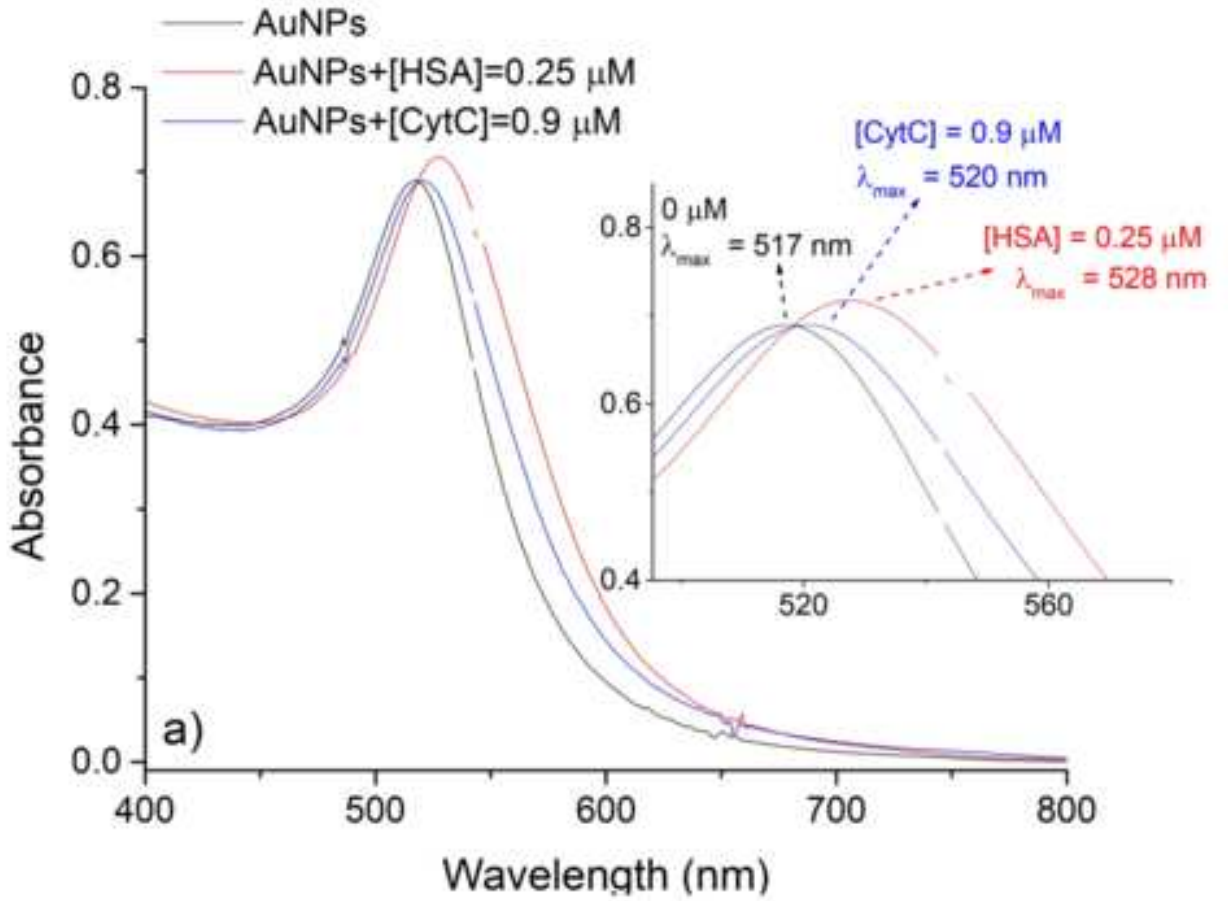

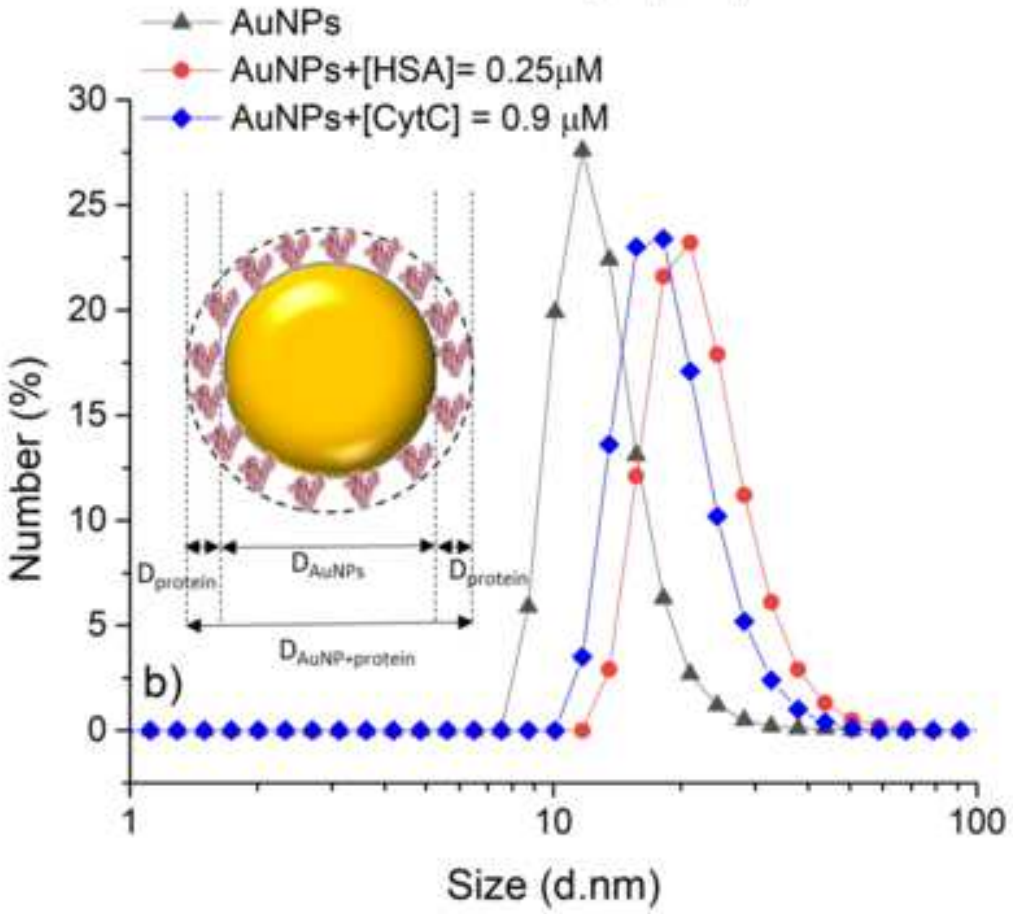

Figure

Click here to access/download;Figure;Fig.2.jpg

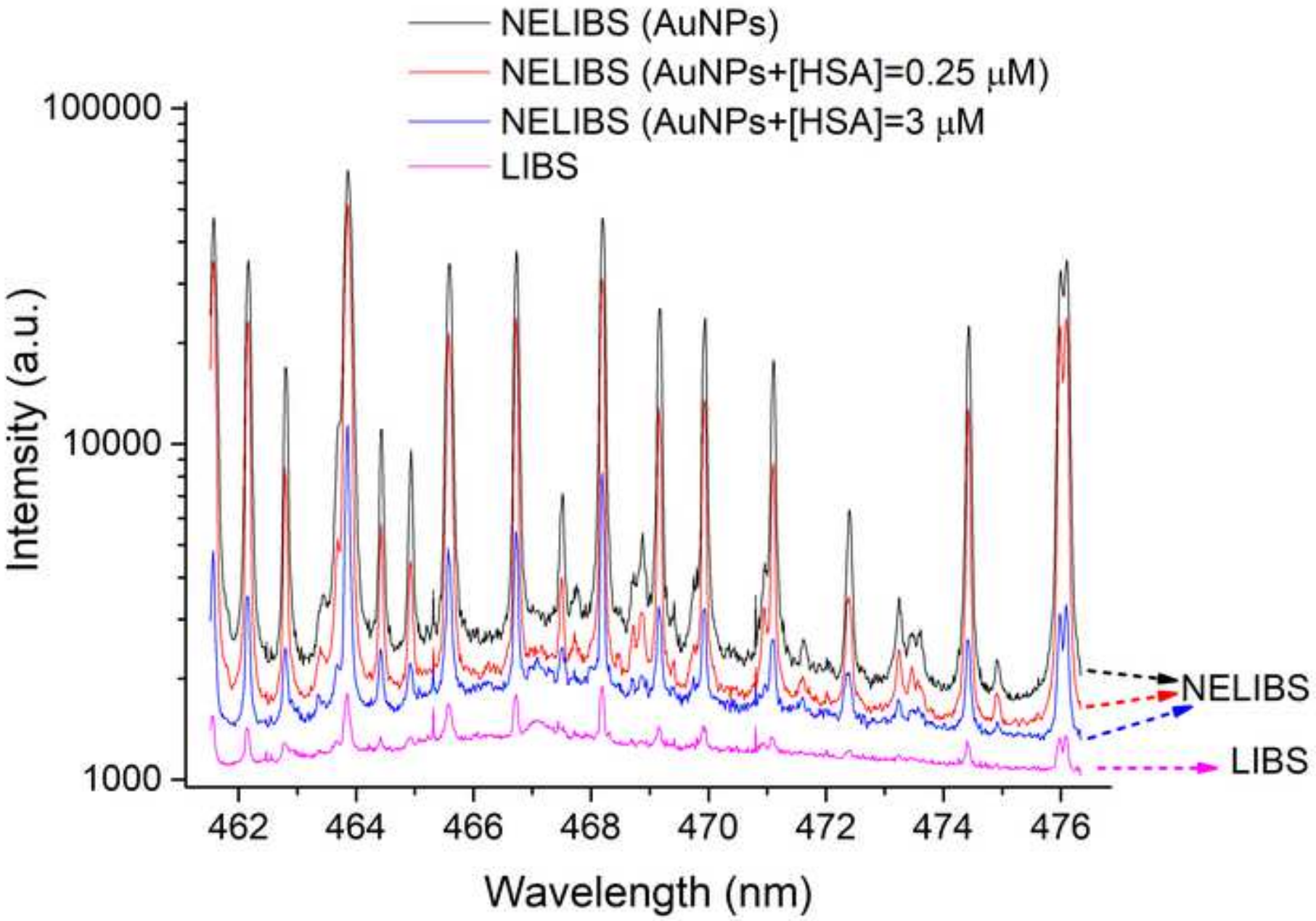

Figure

Click here to access/download;Figure;Fig.3.tif

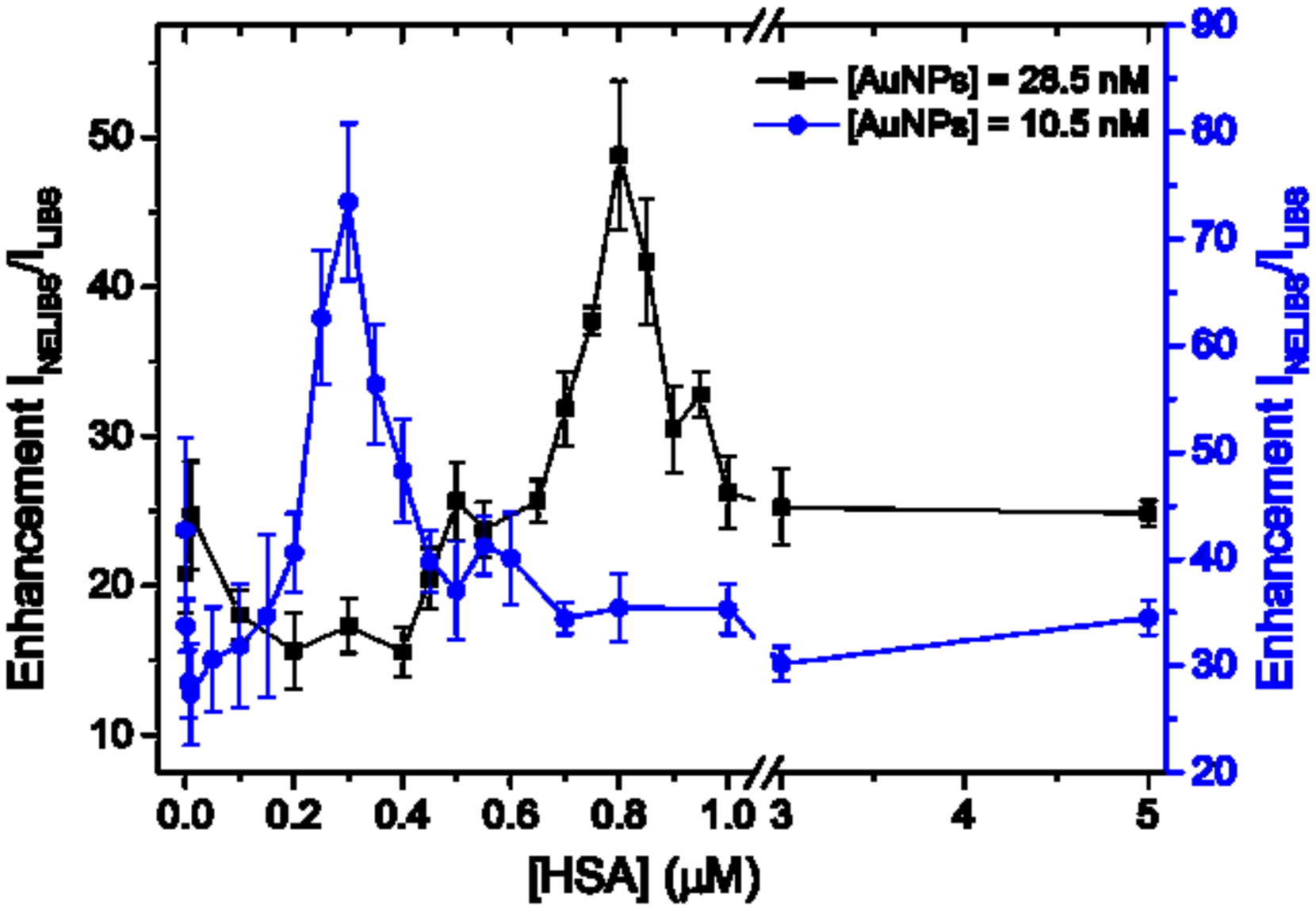

Figure

Click here to access/download;Figure;Fig.4.jpg

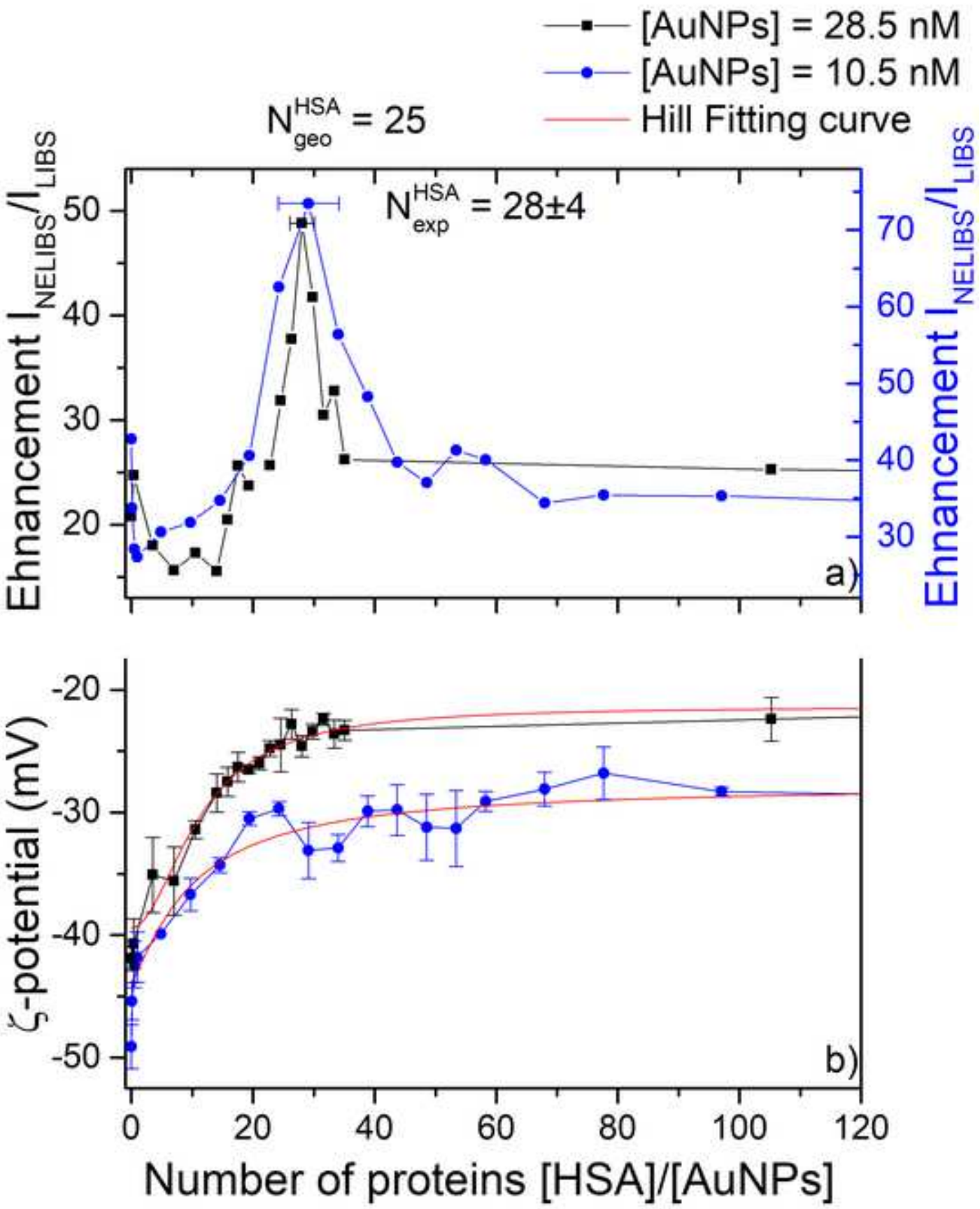

Figure

Click here to access/download;Figure;Fig.5.tif

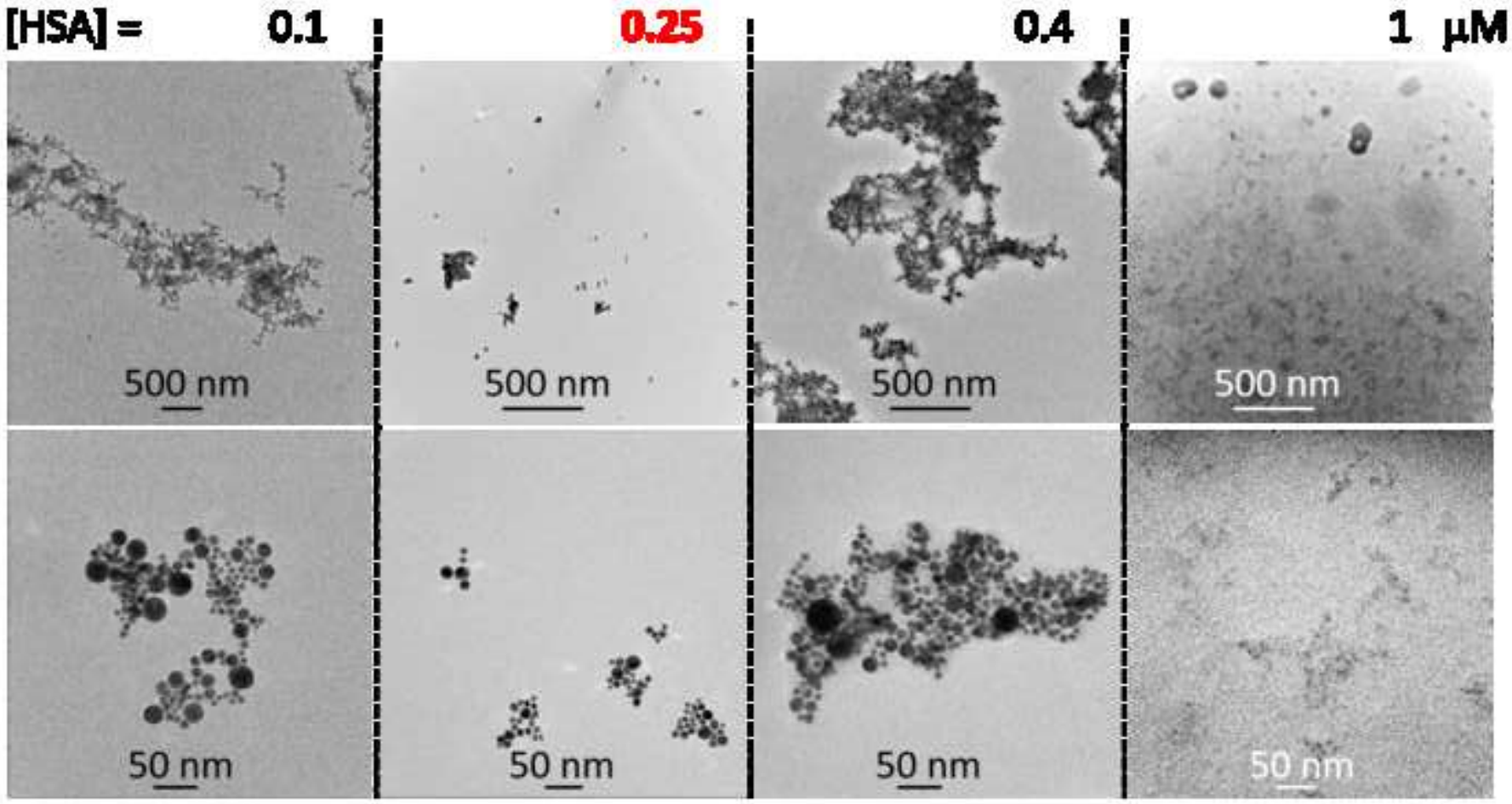

Figure

Click here to access/download;Figure;Fig.6.jpg

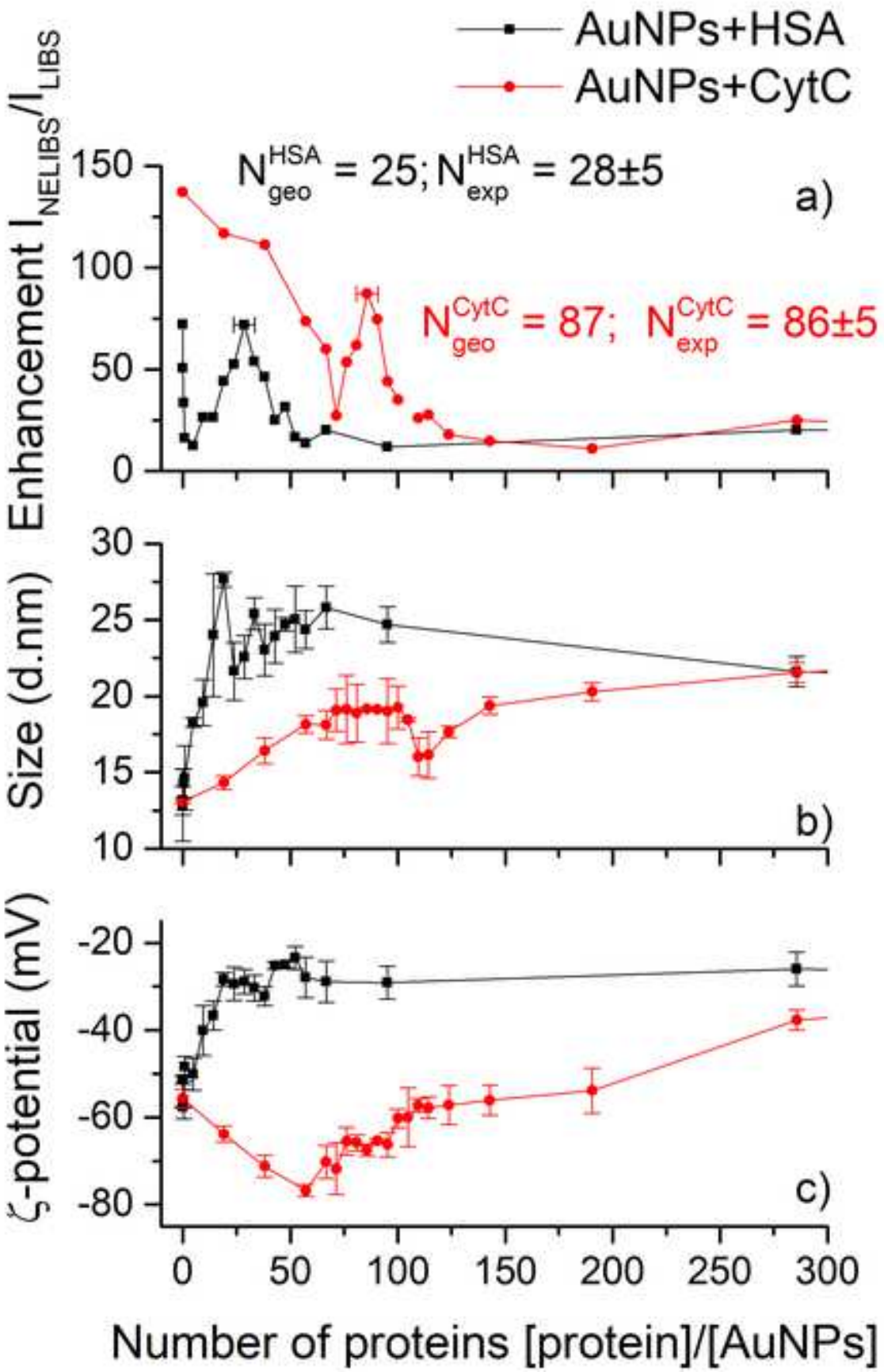

Figure

Click here to access/download;Figure;Fig.7.tif

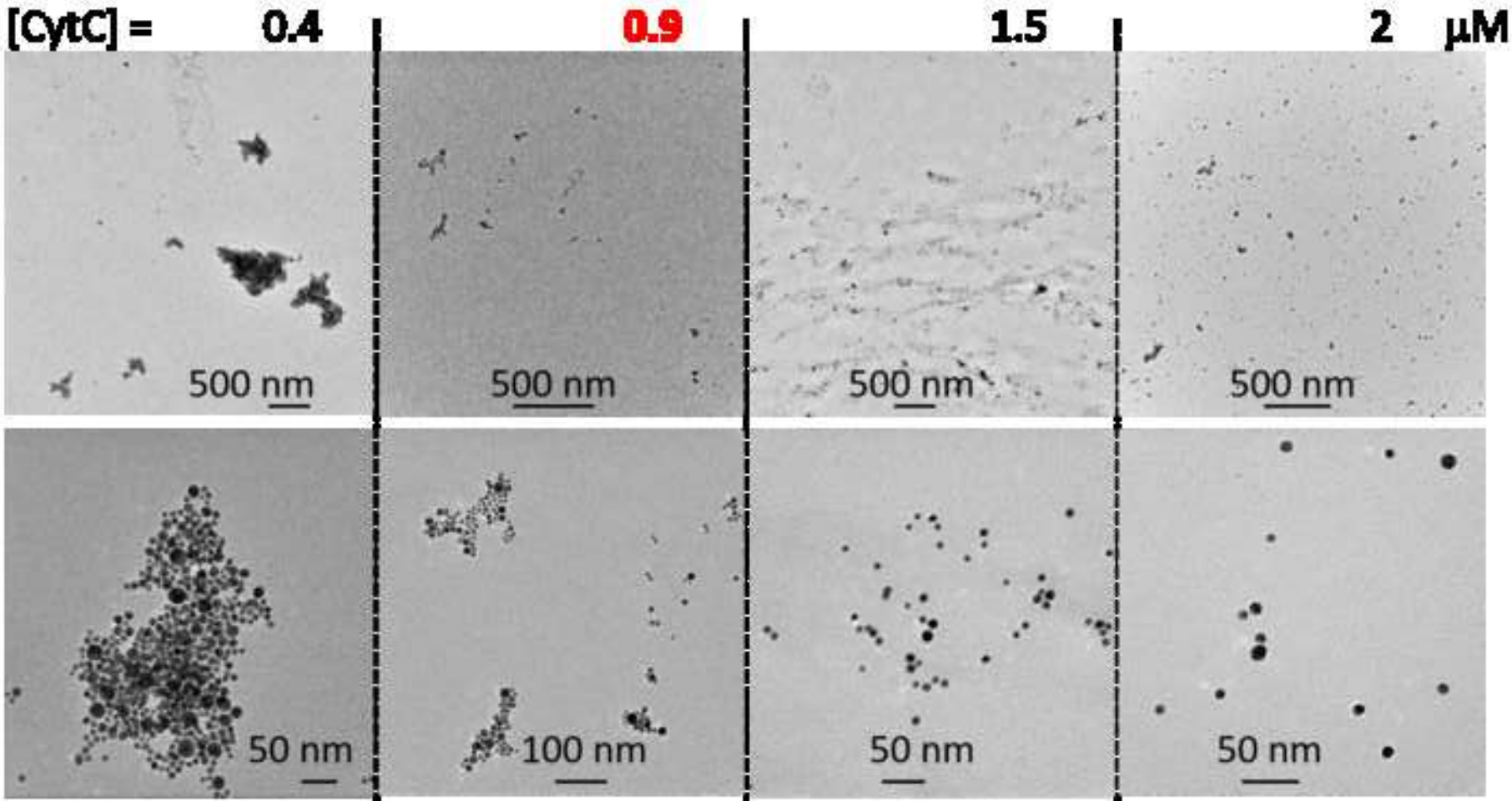

Figure

Click here to access/download;Figure;Fig.8.tif

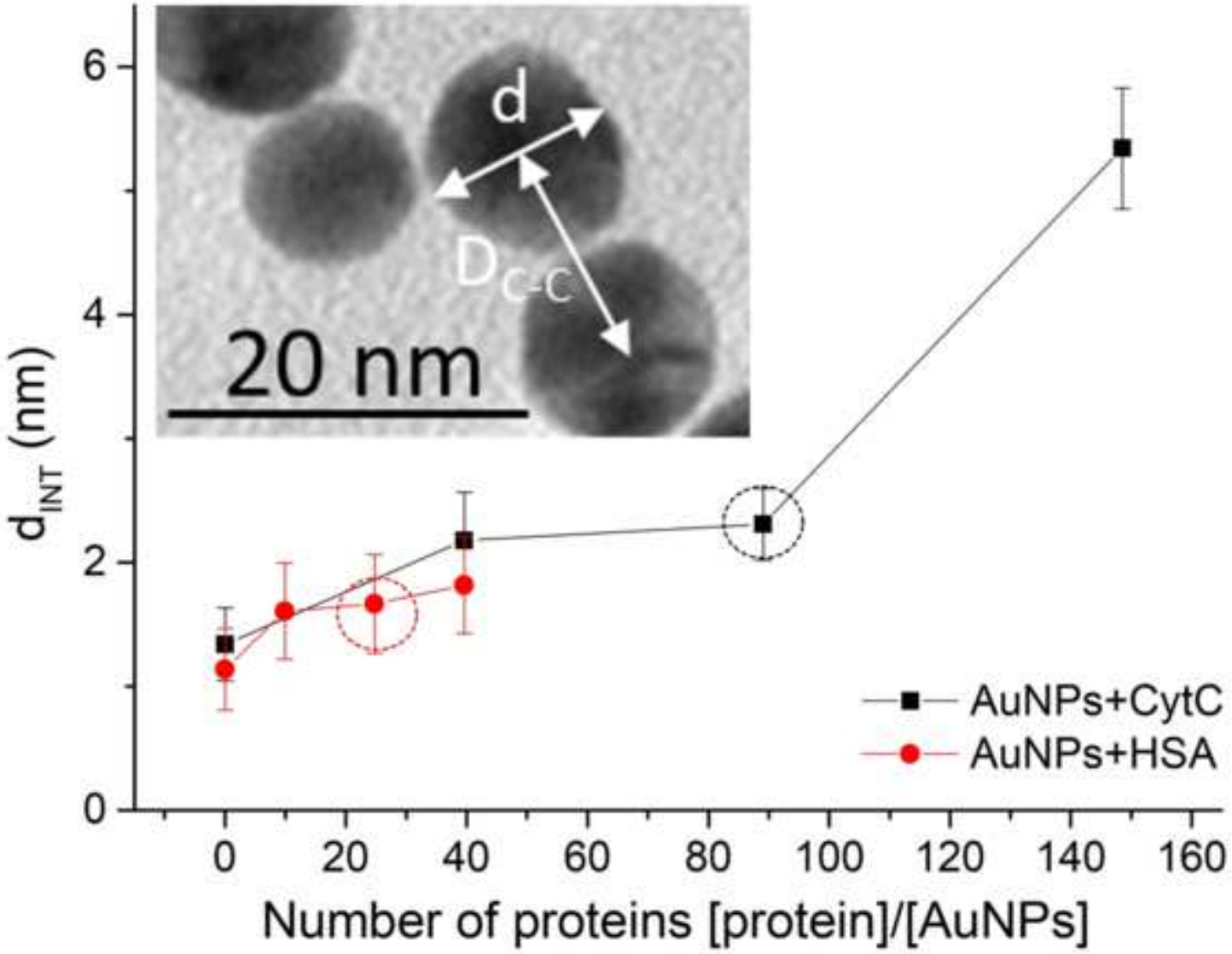

Check list

1) Corresponding authors:

- *(sender to Talanta)* *Dr. Marcella Dell'Aglio*, CNR-NANOTEC, Istituto di Nanotecnologia, c/o Chemistry Department, Via Orabona 4, 70125 Bari, Italy;

marcella.dellaglio@cnr.it

- *Dr. Antonia Mallardi*, CNR-IPCF, Istituto per i Processi Chimico Fisici, c/o Chemistry Department, Via Orabona 4, 70125 Bari, Italy;

a.mallardi@ba.ipcf.cnr.it

2) Cover letter
3) Manuscript:
    - Include keywords
    - All figures (include relevant captions)
    - All tables (including titles, description)
    - References
    - Acknowledgments
4) Graphical Abstracts / Highlights file
5) Supplemental file
6) Referee suggestions
7) Novelty statement
8) Declaration of Interest Statement

List of Three Potential Reviewers

Gábor Galbács
Department of Inorganic and Analytical Chemistry, University of Szeged, Dóm square 7, 6720 Szeged, Hungary

galbx@chem.u-szeged.hu

Tatiana Trejos
Tatiana.trejos@mail.wvu.edu

West Virginia University, Department of Forensic and Investigative Sciences, 208 Oglebay Hall, WV 26506-6121, USA

Yoshihiro Deguchi
Graduate School of Advanced Technology and Science, Tokushima University, Tokushima 770-8501, Japan

ydeguchi@tokushima-u.ac.jp

Declaration of interests

☐ The authors declare that they have no known competing financial interests or personal relationships that could have appeared to influence the work reported in this paper.

Supplementary Material